



1

2 **Development of an improved two-sphere integration technique**  
3 **for quantifying black carbon concentrations in the atmosphere**  
4 **and seasonal snow**

5 **Xin Wang<sup>1,2</sup>, and Xueying Zhang<sup>3</sup>**

6

7 <sup>1</sup> Key Laboratory for Semi-Arid Climate Change of the Ministry of Education, Lanzhou University,

8 Lanzhou 730000, Gansu, China

9 <sup>2</sup> Institute of Surface-Earth System Science, Tianjin University, Tianjin 300072

10 <sup>3</sup> Jilin Weather Modification Office, Changchun 132000, Jilin, China

11

12

13

14

15

16

17

18

19 *Correspondence to:* Xin Wang (Tel: +86 931 8915892)

20 *E-mail address:* [wxin@lzu.edu.cn](mailto:wxin@lzu.edu.cn) (X. Wang)

21

22

23



24 **Abstract.** An improved two-sphere integration (TSI) technique has been developed to  
25 quantify black carbon (BC) concentrations in the atmosphere and seasonal snow. The major  
26 advantage of this system is that it combines two distinct spheres to reduce the scattering  
27 effect due to light-absorbing particles, and thus provides accurate determinations of total  
28 light absorption from BC collected on Nuclepore filters. The TSI technique can be  
29 calibrated using a series of 15 filter samples of standard fullerene soot. This technique  
30 quantifies the mass of BC by separating the spectrally resolved total light absorption into  
31 BC and non-BC fractions. To assess the accuracy of the improved system, an empirical  
32 procedure for measuring BC concentrations by a two-step thermal–optical method is also  
33 applied. Laboratory results indicate that BC concentrations determined using the TSI  
34 technique and theoretical calculations are well correlated, whereas the thermal–optical  
35 method underestimates BC concentrations by 35%–45%. Assessments of the two methods  
36 for atmospheric and snow samples revealed excellent agreement, with least-squares  
37 regression lines with slopes of 1.72 ( $r^2 = 0.67$ ) and 0.84 ( $r^2 = 0.93$ ), respectively. However,  
38 the TSI technique is more accurate in quantifications of BC concentrations in both the  
39 atmosphere and seasonal snow, with an overall lower uncertainty. Using the improved TSI  
40 technique, we find that light absorption due to BC plays a dominant role, relative to non-  
41 BC light absorption, in both the atmosphere (68.5%–95.9% of total light absorption) and  
42 seasonal snow (52.3%–93.3%) over northern China.

43

#### 44 ARTICLE INFO

45 *Keywords:*

46 Black carbon

47 Elemental carbon

48 Light absorption

49 Two-sphere integration technique

50 Thermal–optical method



## 51 1 Introduction

52 Black carbon (BC) has long been recognized as the major light-absorbing particle type  
53 in both natural and anthropogenic emissions (Slater et al., 2002; Koch et al., 2009; Zhang  
54 et al., 2009; Pan et al., 2010; McMeeking et al., 2011; Pavese et al., 2012; Bond et al., 2013;  
55 IPCC, 2013). BC can impact the regional and global climate in several ways, including via  
56 the direct effects of scattering and absorbing visible solar radiation (Jacobson, 2001b;  
57 Menon et al., 2002; Hansen et al., 2005; Ramanathan and Carmichael, 2008), the semi-  
58 direct effects of changing the temperature structure and relative humidity of the atmosphere  
59 by absorbing solar short-wave radiation (Weiss et al., 2012), and indirect effects on cloud  
60 formation and lifetime (Chuang et al., 2002; Baumgardner et al., 2004; Rosenfeld et al.,  
61 2008). Once deposited onto snow or ice surfaces, BC absorbs more solar radiation than  
62 pure snow or ice and reduces the snow albedo, thus accelerating snow melt (Xu et al.,  
63 2009a; Flanner et al., 2012; Hadley and Kirchstetter, 2012; Carmagnola et al., 2013; Qian  
64 et al., 2014; Zhao et al., 2014).

65 Optically classified BC is also often referred to as elemental carbon (EC), which is typically  
66 thermally detected. The distinction between BC and EC has been debated since the 1980s  
67 (Heintzenberg, 1989; Horvath, 1993a; Andreae and Gelencser, 2006; Moosmuller et al.,  
68 2009). Given that BC and EC are both soot particles with diameters of  $<1 \mu\text{m}$ , these terms  
69 have often been used interchangeably (Chow et al., 2001, 2004; Ming et al., 2009;  
70 Thevenon et al., 2009; Lim et al., 2014). BC is generally regarded as ideal light-absorbing  
71 particles of carbon, and is typically measured using optical attenuation methods (Clarke et  
72 al., 1987; Grenfell et al., 2011; Hansen et al., 1984; Ogren and Charlson, 1983). The term  
73 ‘EC’ is often used interchangeably with ‘BC’ when referring to optical absorption  
74 measurements (Clarke et al., 1987; Grenfell et al., 2011), and is only uniquely identified  
75 by thermal–optical methods (Xu et al., 2006; Cao et al., 2007; Jimenez et al., 2009). There  
76 remains poor agreement between measurements of BC and EC among available  
77 measurement techniques. The general techniques used to quantify the various fractions of  
78 BC mass concentrations are associated with the corresponding methods: thermal–optical  
79 methods, single-particle soot photometer (SP2) measurements, and filter-based optical  
80 techniques. Besides the above techniques, the aerosol mass spectrometry, electron



81 microscopy, and Raman spectroscopy are also useful and accurate methods to identify the  
82 various fractions of carbonaceous aerosols in the atmosphere (Cross et al., 2010; Ivleva et  
83 al., 2007; Spencer et al., 2007; Li et al., 2016; Petzold et al., 2013). Among these methods,  
84 the thermal–optical approach is regarded as the most effective and reliable for evaluating  
85 EC concentrations (Chylek et al., 1987; Cachier and Pertuisot, 1994; Jenk et al., 2006;  
86 Legrand et al., 2007; Hadley et al., 2010). However, the thermal–optical method can lead  
87 to large discrepancies in determining EC concentrations as a result of inference from  
88 positive artifacts caused by inadequately separated organics and mineral dust (Ballach et  
89 al., 2001; Wang et al., 2012). Further discrepancies are caused by the use of two main  
90 detection protocols [thermal–optical transmission (TOT) and thermal–optical reflectance  
91 (TOR)] to assess EC and OC concentrations based on their unique thermal properties.  
92 These protocols yield different OC and EC concentrations (Chow et al., 1993, 2001; Birch  
93 and Cary, 1996; Watson and Chow, 2002). The Integrating Sphere/Integrating Sandwich  
94 Spectrophotometer (ISSW) method was developed by Grenfell et al. (2011) and has been  
95 used to analyze mass concentrations of BC in snow (Doherty et al., 2010, 2014; Wang et  
96 al., 2013). Doherty et al. (2010) noted that the total uncertainty in measuring BC in snow  
97 using the ISSW method is up to 40% relative to the gravimetric standards of BC (fullerene  
98 soot). Finally, the SP2 technique is well suited to the quantification of low BC  
99 concentrations with small particle radii (<500 nm). It is an optimized method for measuring  
100 BC concentrations and size distributions, and the substantially larger uncertainty of the SP2  
101 instrument with respect to BC concentration measurements can exceed 60% in snow and  
102 ice cores, and 30% for atmospheric sampling (Schwarz et al., 2012).

103 Although several field campaigns have collected atmospheric, snow, and ice core  
104 samples to measure BC and EC concentrations globally (Wolff and Cachier, 1998; von  
105 Schneidmesser et al., 2009; Doherty et al., 2010, 2014; Ming et al., 2010; Huang et al.,  
106 2011; Xu et al., 2012; Cong et al., 2015), biases remain in determinations of BC  
107 concentrations, as is evident from a comparison among the results obtained with the SP2,  
108 ISSW, and thermal–optical methods (Schwarz et al., 2012; Lim et al., 2014). As a result, it  
109 is difficult to assess the effects of BC and EC on recent climate change using different  
110 techniques, even in the same area.



111 Here we report the development of a new portable and accurate spectrophotometric  
112 method based on the two-sphere integration (TSI) technique that can be used to determine  
113 BC concentrations in both the atmosphere and seasonal snow. The improved TSI technique  
114 minimizes scattering effects related to BC and non-BC insoluble particles collected on  
115 Nuclepore filters, and thus provides a simple and accurate means to assess BC  
116 concentrations in the atmosphere and seasonal snow. To assess the accuracy of the new  
117 technique, a two-step thermal–optical method is applied to determine BC concentrations  
118 on individual quartz fiber filters. Finally, we investigate the spatial distribution of BC  
119 concentrations and the relative light absorption of surface snow over northeast China. We  
120 also analyze the diurnal variations of BC in the atmosphere during day and night over  
121 Lanzhou in northwest China.

## 122 **2 Experimental Procedures**

### 123 **2.1 Sampling sites and snow-sample filtration**

124 During the study period, less snow fell in 2014 than in 2010, and no seasonal snow was  
125 present in the western part of Inner Mongolia. Therefore, we collected 94 snow samples at  
126 14 sites in January and February of 2014 across north China following the sampling route  
127 of Huang et al. (2011). The sites are numbered in chronological order from 90 to 103,  
128 following previous snow surveys (Ye et al., 2012; Wang et al., 2013). Figure 1 shows the  
129 locations of the snow field campaigns across northern China. The sampling locations were  
130 selected to be at least 50 km from any settlement and 1 km from the nearest road. Snow  
131 samples were kept frozen before being filtered. At a temporary laboratory set up along the  
132 sampling route, the snow samples were quickly melted in a microwave. Subsequently, we  
133 simultaneously filtered the snow samples using quartz fiber filters with 1- $\mu\text{m}$  pores and  
134 Nuclepore filters with 0.4- $\mu\text{m}$  pores. Then, we refiltered the snow samples for the quartz  
135 fiber filters using Nuclepore filters with 0.4- $\mu\text{m}$  pores to account for the loss of BC mass  
136 in the 1- $\mu\text{m}$  pore quartz fiber filters. Finally, we stored the original and refiltered snow  
137 samples in clean high-density polyethylene bottles in a freezer at  $-30^{\circ}\text{C}$  for subsequent  
138 analysis. For details of the sampling and filtration procedures, see Wang et al. (2013).

139 To evaluate the accuracy of the TSI technique in measuring BC concentrations, the



140 atmospheric samples were collected continuously on Nuclepore and quartz fiber filters with  
141 high-volume samplers during the periods 09:00 to 17:00 (daytime; local time) and 23:00  
142 to 07:00 (nighttime) at site 103 in Lanzhou from 5 to 25 August 2015. The pumps were  
143 operated at a flow rate of  $10 \text{ L min}^{-1}$ . In total, 40 atmospheric samples were collected during  
144 this experiment and used to assess the accuracy of the atmospheric BC concentration  
145 measurements of the improved TSI technique.

## 146 **2.2 Two-sphere integration technique**

147 Light transmission techniques are the most commonly used methods for determining  
148 light-absorbing impurities in aerosol filter samples of the atmosphere and snow/ice. Since  
149 the 1970s, a series of optical attenuation techniques have been developed for estimating  
150 BC concentrations using light transmission changes through filters, based on Beer's law.  
151 An integrating sphere (IS) technique was first proposed for measuring BC by Fischer  
152 (1970). The integrating sphere was coated with diffusely reflecting white paint through a  
153 small hole, and the reduction in signal after measuring the sample filters represented the  
154 absorption of BC. Subsequently, a new integrating plate (IP) instrument was developed to  
155 measure scavenging BC on filters based on the IS technique, which uses a light-diffusing  
156 support to provide a nearly Lambertian light source for light transmission using  $0.4\text{-}\mu\text{m}$   
157 Nuclepore filters (Clarke et al., 1987; Horvath, 1993b). However, the multiple scattering  
158 of solar radiation affect the accuracy of the IP technique (Clarke et al., 1987; Hitzemberger,  
159 1993; Petzold et al., 1997; Bond et al., 1999). A new integrating-sandwich configuration  
160 of the ISSW instrument was designed to measure the absorption of light-absorbing  
161 impurities based on the ISSW principle of Grenfell et al. (2011). The ISSW instrument can  
162 isolate the absorption properties of light-absorbing impurities deposited on polycarbonate  
163 Nuclepore filters. By assuming the mass absorption efficiency and non-BC Ångström  
164 exponent at 550 nm, this technique is currently capable of reliably measuring BC and non-  
165 BC light absorption (Wang et al., 2013; Dang and Hegg, 2014; Doherty et al., 2014).  
166 However, Schwarz et al. (2012) found that the total instrumental uncertainty associated  
167 with ISSW BC concentration determinations for ambient snow is 11%, and that this  
168 uncertainty is partially due to the scattering effects of insoluble impurities deposited on the  
169 filters (Doherty et al., 2010; Grenfell et al., 2011).



170 The improved TSI spectrophotometer developed in this study is small, lightweight, and  
171 portable, and can accurately quantify BC concentrations using a technique based on the  
172 integrating sphere and integrating plate transmission techniques (Fig. 2). The major  
173 improvement of this spectrophotometer is that we replaced the integrating sandwich of the  
174 ISSW instrument developed by Grenfell et al. (2011) with a new integrating sphere. In  
175 addition, an iron hoop is applied to the top integrating sphere surrounding the sapphire  
176 windows to reduce light scattering due to insoluble particles on the filters. Therefore, the  
177 total relative light absorption due to all insoluble impurities on the filter can be estimated  
178 from the visible-to-near-infrared wavelengths. The total light attenuation can be calculated  
179 from the light transmitted by a snow or atmospheric sample,  $S(\lambda)$ , compared with that  
180 transmitted by a blank filter,  $S_0(\lambda)$ . Then, the relative attenuation ( $A_{tn}$ ) through the filter  
181 can be expressed as follows

$$182 \quad A_{tn} = -\ln[S(\lambda)/S_0(\lambda)] \quad (1)$$

183 Then, the total absorption Ångström exponent  $\mathring{A}_{tot}(\lambda_0)$  of all the ILAPs on the filters  
184 can be calculated from the following formula:

$$185 \quad \mathring{A}_{tot}(\lambda_0) = -\frac{\ln[\tau_{tot}(\lambda_1)/\tau_{tot}(\lambda_2)]}{\ln(\lambda_1/\lambda_2)} \quad (2)$$

186  $\mathring{A}_{non-BC}$  is calculated as a linear combination of the contributions to light absorption  
187 made by OC and Fe:

$$188 \quad \mathring{A}_{non-BC} = \mathring{A}_{OC} \times f_{OC} + \mathring{A}_{Fe} \times f_{Fe} \quad (3)$$

189 The total absorption Ångström exponent of all ILAPs on a filter ( $\mathring{A}_{tot}$ ) can be described  
190 as a linear combination of  $\mathring{A}_{BC}$  and  $\mathring{A}_{non-BC}$  weighted by the light absorption fraction:

$$191 \quad \mathring{A}_{tot}(\lambda_0) = \mathring{A}_{BC} \times f_{BC}(\lambda_0) + \mathring{A}_{non-BC} \times f_{non-BC}(\lambda_0) \quad (4)$$

192 Using the mass absorption efficiency and absorption Ångström exponents for BC, OC,  
193 and Fe described by Wang et al. (2013), we can further estimate the following parameters:  
194 equivalent BC ( $C_{BC}^{equiv}$ ), maximum BC ( $C_{BC}^{max}$ ), estimated BC ( $C_{BC}^{est}$ ), fraction of light  
195 absorption by non-BC ILAPs (insoluble light-absorbing particles) ( $f_{non-BC}^{est}$ ), absorption  
196 Ångström exponent of non-BC ILAPs ( $\mathring{A}_{non-BC}$ ), and total absorption Ångström exponent  
197 ( $\mathring{A}_{tot}$ ). These parameters are defined as follows.

198 1.  $C_{BC}^{equiv}$  ( $\text{ng g}^{-1}$ ): *equivalent BC* is the amount of BC that would be needed to produce the  
199 total light absorption by all insoluble particles in snow for wavelengths of 300–750 nm.



- 200 2.  $C_{BC}^{max}$  ( $\text{ng g}^{-1}$ ): *maximum BC* is the maximum possible BC mixing ratio in snow,  
201 assuming that all light absorption is due to BC at wavelengths of 650–700 nm.
- 202 3.  $C_{BC}^{est}$  ( $\text{ng g}^{-1}$ ): *estimated BC* is the estimated true mass of BC in snow derived by  
203 separating the spectrally resolved total light absorption and non-BC fractions.
- 204 4.  $f_{non-BC}^{est}$  (%): the *fraction of light absorption by non-BC light-absorbing particles* is the  
205 integrated absorption due to non-BC light-absorbing particles. This value is weighted by  
206 the down-welling solar flux at wavelengths of 300–750 nm.
- 207 5.  $\dot{A}_{non-BC}$ : the *non-BC absorption Ångström exponent* is derived from the light absorption  
208 by non-BC components for wavelengths of 450–600 nm.
- 209 6.  $\dot{A}_{tot}$ : the *absorption Ångström exponent* is calculated for all insoluble particles deposited  
210 on the filter between 450 and 600 nm.

211 Furthermore, combining with the mass loading of Fe was determined by chemical  
212 analysis (Wang et al., 2013), the mass loading of OC ( $L_{OC}$ ) was also estimated assuming  
213 that the mass absorption coefficient (MAC) for OC is  $0.3 \text{ m}^2 \text{ g}^{-1}$  at the wavelength of 550  
214 nm using the following equation:

$$215 \quad \tau_{tot}(\lambda) - MAC_{BC}(\lambda) \times L_{BC}^{est} - MAC_{Fe} \times L_{Fe} = MAC_{OC} \times L_{OC} \quad (5)$$

216 All relevant equations and associated derivations are described by Grenfell et al. (2011)  
217 and Doherty et al. (2010, 2014). Note that the calculation of non-BC light absorption due  
218 to insoluble impurities assumes that the iron in snow is predominantly from mineral dust  
219 (Wang et al., 2013).

### 220 2.3 Calibration of the TSI spectrophotometer

221 In this study, a series of 15 Nuclepore filters with a pore size of  $0.2 \mu\text{m}$  (LOT# 7012284,  
222 25mm, Whatman) loaded with fullerene soot (stock #40971, lot #L20W054, Alfa Aesar,  
223 Ward Hill, MA, USA) is used to calibrate the spectrophotometer over the range 0.63–38.6  
224  $\mu\text{g}$ , which typically covers >75% of ambient accumulation mode mass (left panel in Table  
225 1; Schwarz et al., 2012). Fullerene soot is commonly used for calibrating the light  
226 transmission and thermal–optical techniques for measuring BC concentrations  
227 (Baumgardner et al., 2012). Standard fullerene soot particles are fractal-like aggregates of  
228 spherical primary particles with a diameter of  $\sim 50 \text{ nm}$ , with a mean density of  $1.05 \text{ g cm}^{-3}$





229 (Moteiki et al., 2009). Multiple filters with various loadings are required, as the system  
230 response deviates from Beer's law exponential behavior; related equations can be found in  
231 Grenfell et al. (2011). Note that uncertainties in mass absorption efficiencies, which range  
232 from 2 to 25 m<sup>2</sup> g<sup>-1</sup>, can lead to uncertainty in this technique. Here, we use a mass  
233 absorption efficiency of 6.22 m<sup>2</sup> g<sup>-1</sup> at 525 nm, which is consistent with Doherty et al. (2010)  
234 and Grenfell et al. (2011). Figure 2 shows the best-fit curve (solid line) of loading of the  
235 filters at 550 nm. When the filter loading was 0–40 μg cm<sup>-2</sup>, all measured results were close  
236 to the best-fit curve, indicating that the TSI spectrophotometer is stable and accurate in  
237 terms of BC mass measurements.

#### 238 **2.4 Thermal–optical measurements of EC concentration**

239 There are several types of thermal–optical method that can be used to quantify EC and  
240 OC concentrations, including two-step temperatures in oxidizing/non-oxidizing  
241 atmospheres (Cachier et al., 1989; Xu et al., 2006, 2009b), thermal–optical reflectance  
242 (Chow et al., 1993, 2001; Chen et al., 2004), and thermal–optical transmittance (Sharma et  
243 al., 2002; Yang and Yu, 2002; Chow et al., 2004). Using an optimized two-step method,  
244 Cachier et al. (1989) first confirmed that soot carbon not only comprises EC, but is also  
245 mixed with highly condensed organic material. An optimized two-step thermal–optical  
246 system has been developed to detect EC and OC concentrations in ice cores (Xu et al.,  
247 2006). Here, we use the optimized two-step method based on the thermal–optical technique  
248 to measure EC concentrations. In this experiment, quartz fiber filters were first preheated  
249 in a muffle furnace at 350°C to remove organic carbon prior to sampling. All filters were  
250 punched to yield appropriately sized samples for analysis. Snow samples were analyzed  
251 for EC and OC concentrations using a Thermal–Optical Carbon Analyzer (Desert Research  
252 Institute, Model 2001A), following the thermal–optical reflectance (TOR) protocol of the  
253 Interagency Monitoring of Protected Visual Environments (IMPROVE\_A). We developed  
254 a new method, referred to as the two-step method, to measure the concentrations of BC  
255 collected by the quartz fiber filters. The two-step method is an updated measurement  
256 procedure that first extracts an OC fraction below 550°C in a He atmosphere. The  
257 volatilized OC is oxidized to CO<sub>2</sub>, reduced to CH<sub>4</sub>, and detected by a flame ionization  
258 system. Next, two EC fractions (EC1 and EC2) are extracted above 550°C in an atmosphere



259 of 2% O<sub>2</sub> and 98% He. Detailed procedures can be found in Xu et al. (2006) and Chow et  
260 al. (2004). The analytical uncertainty of this method is 15% for BC and 16% for OC (Xu  
261 et al., 2009).

## 262 **3 Results**

### 263 **3.1 Comparison with theoretical calculations**

264 To further assess the accuracy of the TSI system, we use standard fullerene soot and  
265 quantify BC concentrations using theoretical calculations for comparison with BC values  
266 measured by a laboratory-based TSI spectrophotometer. To ensure the stability and  
267 accuracy of the improved TSI spectrophotometer, two individual sets of standard BC filters  
268 were used: 0.4- $\mu\text{m}$  Nuclepore and 1- $\mu\text{m}$  quartz fiber filters. All filters were preheated in a  
269 muffle furnace at 350°C to remove organic carbon prior to sampling. A measured amount  
270 of BC was mixed into a known volume of ultrapure water. The mixture was then agitated  
271 by ultrasound for ~10 min, and the same volumes of liquid were then filtered through the  
272 two types of filter. Using the calculated BC mass, seven filters with gradually increasing  
273 BC concentrations were obtained for both the 0.4- $\mu\text{m}$  Nuclepore and 1- $\mu\text{m}$  quartz fiber  
274 filters. Next, all the filters were placed in a dryer for 24 h and then measured using the TSI  
275 spectrophotometer. Using the BC mass and the volume of the ultrapure water used for  
276 filtration, we can estimate the theoretical BC concentration for each filter. The mass for  
277 each filter is listed in Table 1 (right panel).

278 Assuming a mass absorption cross-section (MAC) of BC of 6.22 m<sup>2</sup> g<sup>-1</sup> at 525 nm, the  
279 BC concentrations measured using the TSI spectrophotometer were in good agreement  
280 with the theoretical BC values (slope of 1.07). The BC mass loaded on the Nuclepore filters  
281 was approximately equal to that measured by the improved TSI spectrometer, which  
282 indicates that the TSI system developed here can accurately measure BC concentrations  
283 with the assumed mass absorption efficiency. In contrast, the standard BC mass on the  
284 quartz fiber filters was underestimated by 35%–45% using the two-step thermal–optical  
285 technique, compared with the theoretical value. During the filtration process, we found that  
286 the time required to filter liquid snow samples on the 0.4- $\mu\text{m}$  Nuclepore filters was much  
287 longer than was the case for the 1- $\mu\text{m}$  quartz fiber filters. Therefore, we first filtered the



288 melted snow samples on the quartz fiber filters, and then re-filtered the snow samples using  
289 the 0.4- $\mu\text{m}$  Nuclepore filters. Using this process, BC mass losses can be obtained using the  
290 TSI technique, assuming optical BC is equivalent to thermal EC.

291 As shown in Figure 5, the fraction of BC mass collected during the second filtration (0.4-  
292  $\mu\text{m}$  filter) ranges from 12% to 21% of the total collected mass ( filter directly with 0.4- $\mu\text{m}$   
293 filters), as might be expected for the small particles of standard fullerene soot (<50 nm).  
294 This under-sampled fraction decreases with increasing BC mass on the filters, possibly  
295 owing to blocking of the filter pores. As a result, the under-sampled fraction of the thermal-  
296 optical method was larger than that of the TSI technique, leading to a lower filtration  
297 efficiency. Note that these sampling efficiencies are strongly related to the BC size  
298 distribution. Therefore, the improved TSI technique developed here is more stable and  
299 accurate for measuring pure BC masses, and the data obtained using this method can be  
300 used as the standard BC mass. After correcting for systematic biases, the results of both  
301 methods were closer to the theoretical BC calculations. Note, however, that the size  
302 distribution of the laboratory BC standard was much smaller than those of the atmospheric  
303 and seasonal snow samples (Schwarz et al., 2012). Therefore, underestimates caused by  
304 the filtration efficiency for ambient BC should be lower than that for the standard BC.

### 305 **3.2 Comparison of BC concentrations in seasonal snow and the atmosphere**

306 Recent studies have indicated that mineral dust can affect the accurate detection of BC  
307 concentrations using the ISSW and thermal-optical methods (Wang et al., 2012; Zhou et  
308 al., 2017). To eliminate the large uncertainty and bias due to dust particles, we only used  
309 snow samples collected in industrial areas over northeastern China, where the light  
310 absorption was dominated by fine-mode ILAPs (e.g., BC and OC; Wang et al., 2013).  
311 Hence, most of the snow samples did not contain very large coarse-mode particles, such as  
312 mineral and local soil dust.

313 During the snow field campaign, two series of snow samples were filtered through the  
314 Nuclepore and quartz fiber filters and measured using the TSI and two-step thermal-optical  
315 methods (Fig. 6). Result shows that most of the BC values measured by the TSI and two-  
316 step thermal-optical methods are close to the 1:1 line in a comparison plot, and are  
317 generally in good agreement (slope of 1.11,  $R^2 = 0.93$ ,  $n = 22$ ). However, some BC values



318 in seasonal snow measured by the two-step thermal–optical method are much larger than  
319 those measured by the TSI technique. Consequently, for each sample the mean ratio of BC  
320 concentrations measured by the two-step method and the TSI spectrophotometer varies  
321 from 0.64 to 3.97, with an overall mean of 1.57. This discrepancy arises from two factors.  
322 First, Wang et al. (2017) found that snow grain sizes varied considerably (from 0.07 to 1.3  
323 mm) during this snow field campaign. This range is much larger than that recorded in  
324 previous studies, owing to snow melting by solar radiation and ILAPs (Hadley and  
325 Kirchstetter, 2012; Painter et al., 2013; Yasunari et al., 2013; Pedersen et al., 2015). These  
326 results agree well with those of Schwarz et al. (2012), who found that the sizes of BC  
327 particles in snow are much larger than those in typical ambient air. Therefore, the sampling  
328 efficiency of the quartz fiber filters could have been significantly higher than expected.  
329 The other factor is that the insoluble light-absorbing impurities in seasonal snow over  
330 northeast China contained not only BC, but also insoluble organic carbon. This result is  
331 consistent with a previous study by Chow et al. (2004), who reported that the charring  
332 observed when employing the two-step thermal–optical method at higher temperatures  
333 ( $>550^{\circ}\text{C}$ ) was incomplete and that certain organic compounds are not completely  
334 pyrolyzed below  $550^{\circ}\text{C}$ . Therefore, incomplete charring of absorbed organic compounds  
335 by the two-step processes may lead to incompletely pyrolyzed OC on the filters, artificially  
336 contributing to the BC concentration. This may explain why the BC concentration  
337 measured using the thermal–optical method was higher than that measured using the TSI  
338 spectrophotometer.

339 A comparison of BC concentrations in the atmosphere measured by the ISSW and  
340 thermal–optical methods is vastly different than that for the snow samples (Fig. 7). Results  
341 are in excellent agreement for BC concentrations of  $<3\ \mu\text{g m}^{-3}$ . However, biases increased  
342 gradually with increasing BC concentrations, leading to two-step-to-TSI ratios as low as  
343 0.5. The BC concentrations of  $>3\ \mu\text{g m}^{-3}$  obtained using the two-step thermal–optical  
344 method are much lower than those measured using the improved TSI technique, possibly  
345 due to the small particle sizes in the atmosphere, which lead to a lower filtration efficiency.  
346 Overall, we conclude that the improved TSI method is more stable and suitable for  
347 measuring BC concentrations in both the atmosphere and snow samples compared with the  
348 two-step thermal–optical method.



349 **3.3 Spatial distribution of BC and non-BC light absorption measured by the TSI**  
350 **spectrophotometer**

351 The above results show that the improved TSI method measures BC concentrations in  
352 the atmosphere and snow/ice with higher accuracy than Two-step thermal optical methods.  
353 In this section we investigate the spatial distribution of BC concentrations and their relative  
354 light absorption due to BC and non-BC snow impurities in seasonal snow over northeast  
355 China during January–February 2014. All BC mass concentrations in surface snow  
356 measured by the TSI and thermal–optical methods during the snow field campaigns are  
357 listed in Table 2. There was less snow fall in January 2014 than in 2010, and seasonal snow  
358 did not cover all of central Inner Mongolia during this time. Thus, we only collected snow  
359 samples at site 90. Given that this region is windy, the surface snow collected included  
360 drifted and aged snow. The surface BC concentration was  $350 \text{ ng g}^{-1}$  in the central Inner  
361 Mongolia region. The lowest BC concentrations in surface snow, 55 and  $280 \text{ ng g}^{-1}$ , were  
362 found on the border of northeast China (sites 91–97). We note that there were considerable  
363 variations in BC concentrations in these regions. The median BC concentration was  $1100$   
364  $\text{ng g}^{-1}$  with a range of  $520\text{--}3900 \text{ ng g}^{-1}$  for surface snow in northeast industrial regions. On  
365 10 February 2014, fresh snow samples were collected in Lanzhou, at a mean snow depth  
366 of 6–8 cm. The mean BC concentration in these fresh snow samples from Lanzhou was  
367  $\sim 170 \text{ ng g}^{-1}$ .

368 The relative light absorption due to BC and non-BC fractions in seasonal snow measured  
369 using the improved TSI technique across northern China is shown in Figure 8. A similar  
370 pattern for the light absorption of BC ( $\sim 80\%$ ) and non-BC ( $\sim 20\%$ ) from insoluble light-  
371 absorbing impurities in surface snow indicates a similar pollution emission source over  
372 northeast China. However, the light absorption due to BC in seasonal snow plays a  
373 dominant role (52.3%–93.3%, with a mean of 75.8%). The largest BC light absorption was  
374 at site 102. This site is located in the central part of Jilin province, which is polluted by  
375 heavy industrial activity. For one sample, the light absorption of non-BC impurities in  
376 seasonal snow reached 52.3%, which is the only time it exceeded BC light-absorption.  
377 Biomass burning and fossil fuel are likely the major emission sources during the winter in  
378 Lanzhou, unlike the case over northeast China. These results are consistent with those of



379 Wang et al. (2013), who found that snow particle light absorption was dominated by BC in  
380 northeast China in 2010.

381 Finally, we investigate atmospheric BC mass concentrations and their relative light  
382 absorption measured by the TSI spectrophotometer in Lanzhou during 5–25 August 2015.  
383 During this experiment, there were no noticeable trends of BC concentrations in Lanzhou.  
384 However, a notable feature in Figure 9 is that the BC mass concentrations at night are  
385 generally much higher than during the day (Table 3). The unique topography of Lanzhou  
386 likely plays an important role in this phenomenon. Lanzhou is situated in a valley basin  
387 with low rainfall, high evaporation, low wind speeds, and high calm-wind frequency,  
388 which often leads to a thick inversion layer in which air pollutants accumulate during the  
389 night. The light absorption due to BC in the atmosphere ranges from 68.5% to 93.29%,  
390 with a mean of 77.9%.

#### 391 **4 Conclusions**

392 We developed an improved two-sphere integration (TSI) spectrophotometer to quantify  
393 BC concentrations in snow and atmospheric samples over northern China. The TSI  
394 technique significantly reduces scattering effects caused by insoluble impurities deposited  
395 on filters. Therefore, the system more accurately measures light absorption due to BC and  
396 non-BC impurities. A system calibration using theoretical calculations for standard  
397 fullerene soot revealed that the TSI system can be used to assess BC concentrations with  
398 low uncertainty. A laboratory comparison revealed that the thermal–optical method can  
399 lead to a significant underestimate (35%–45%) of BC concentrations for small-diameter  
400 particles (~50 nm) due to the low filtration efficiency of 1- $\mu$ m quartz fiber filters.

401 To further assess the accuracy of the improved TSI system, two field campaigns were  
402 carried out to collect seasonal snow and atmospheric samples during January–February  
403 2014 and 5–25 August 2015 across northern China, respectively. Although the BC  
404 concentrations measured by the TSI and thermal–optical methods are well correlated for  
405 both the snow and atmospheric samples, we find that some BC values in seasonal snow  
406 measured by the two-step thermal–optical method were significantly overestimated  
407 compared with those measured by the TSI technique, by a factor of 1.57. Overall, the



408 improved TSI optical system developed here is applicable to quantifications of BC  
409 concentrations in the atmosphere and snow/ice.

410 The spatial distribution of BC concentrations in seasonal snow over northern China  
411 during January–February 2014 ranged from 60 to 3800 ng g<sup>-1</sup>, with a mean value of 700  
412 ng g<sup>-1</sup>, and ranged from 0.78 to 7.75 µg m<sup>-3</sup> in the atmosphere during 5–25 August 2015  
413 in Lanzhou. The spatial distribution of BC concentrations shows that large BC values are  
414 found mainly in the center of industrial regions near the central part, whereas lower values  
415 are found in northeast China. Light absorption is dominated by BC (~50% to 95%) in  
416 seasonal snow over northeast China, and this plays a dominant role in accelerating snow  
417 melt. Atmospheric samples collected in Lanzhou show significant changes in BC  
418 concentrations between day and night. Frequent, stable atmospheric boundary layers at  
419 night during summer, caused by the valley-basin topography of Lanzhou, are largely  
420 responsible for air pollutant accumulation during the night.

421  
422  
423  
424

425 *Data availability.* Data used in this paper are available upon request from corresponding  
426 author (wxin@lzu.edu.cn).

427 *Author contributions.* The conceptualization and methodology were done by XW. The  
428 experiments were designed by XZ. The formal analysis, investigation, writing of the  
429 original draft, and editing were performed by XW.

430 *Competing interests.* The authors declare that they have no conflict of interest.

431 *Acknowledgements.* We thank Thomas C. Grenfell and Qiang Fu from University of  
432 Washington for providing the standard filters.

433 *Financial support.* This research was supported by the National Key Research and  
434 Development Program on Monitoring, Early Warning and Prevention of Major Natural



435 Disaster (2018YFC1506005), the National Natural Science Foundation of China  
436 (41775144, 41675065, and 41875091), and the Fundamental Research Funds for the  
437 Central Universities (lzujbky-2018-k02).

438

439

#### 440 **References**

441 Andreae, M.O. and Gelencser, A.: Black carbon or brown carbon? The nature of light-  
442 absorbing carbonaceous aerosols, *Atmos. Chem. Phys.*, 6, 3131-3148, doi:  
443 10.5194/acp-6-3131-2006, 2006.

444 Ban-Weiss, G.A., Cao, L., Bala, G., and Caldeira, K.: Dependence of climate forcing and  
445 response on the altitude of black carbon aerosols, *Clim. Dyn.*, 38, 897-911, doi:  
446 10.1007/s00382-011-1052-y, 2012.

447 Ballach, J., Hitznerberger, R., Schultz, E., and Jaeschke, W.: Development of an improved  
448 optical transmission technique for black carbon (BC) analysis, *Atmos. Environ.*, 35,  
449 2089-2100, doi: 10.1016/S1352-2310(00)00499-4, 2001.

450 Baumgardner, D., Kok, G., and Raga, G.: Warming of the Arctic lower stratosphere by  
451 light absorbing particles, *Geophys. Res. Lett.*, 31, doi: 10.1029/2003GL018883,  
452 2004.

453 Baumgardner, D., Popovicheva, O., Allan, J., Bernardoni, V., Cao, J., Cavalli, F., Cozic, J.,  
454 Diapouli, E., Eleftheriadis, K., Genberg, P.J., Gonzalez, C., Gysel, M., John, A.,  
455 Kirchstetter, T.W., Kuhlbusch, T.A.J., Laborde, M., Lack, D., Muller, T., Niessner, R.,  
456 Petzold, A., Piazzalunga, A., Putaud, J.P., Schwarz, J., Sheridan, P., Subramanian, R.,  
457 Swietlicki, E., Valli, G., Vecchi, R., and Viana, M.: Soot reference materials for  
458 instrument calibration and intercomparisons: a workshop summary with  
459 recommendations, *Atmos. Meas. Tech.*, 5, 1869-1887, doi: 10.5194/amt-5-1869-  
460 2012, 2012.

461 Birch, M.E.: Analysis of carbonaceous aerosols: interlaboratory comparison, *Analyst*  
462 123, 851-857, doi: 10.1039/A800028J, 1998.





- 463 Birch, M. E., and Cary, R. A.: Elemental carbon-based method for monitoring  
464 occupational exposures to particulate diesel exhaust, *Aerosol Sci. Technol.*, 25, 221-  
465 241, doi: 10.1080/02786829608965393, 1996.
- 466 Bond, T.C., Bussemer, M., Wehner, B., Keller, S., Charlson, R.J., and Heintzenberg, J.:  
467 Light absorption by primary particle emissions from a lignite burning plant,  
468 *Environ. Sci. Technol.*, 33, 3887-3891, doi: 10.1021/es9810538, 1999.
- 469 Bond, T.C., Streets, D.G., Yarber, K.F., Nelson, S.M., Woo, J.H., and Klimont, Z.: A  
470 technology-based global inventory of black and organic carbon emissions from  
471 combustion, *J. Geophys. Res.-Atmos.*, 109, doi:10.1029/2003JD003697, 2004.
- 472 Bond, T.C., Doherty, S.J., Fahey, D.W., Forster, P.M., Berntsen, T., DeAngelo, B.J., Flanner,  
473 M.G., Ghan, S., Karcher, B., Koch, D., Kinne, S., Kondo, Y., Quinn, P.K., Sarofim, M.C.,  
474 Schultz, M.G., Schulz, M., Venkataraman, C., Zhang, H., Zhang, S., Bellouin, N.,  
475 Guttikunda, S.K., Hopke, P.K., Jacobson, M.Z., Kaiser, J.W., Klimont, Z., Lohmann, U.,  
476 Schwarz, J.P., Shindell, D., Storelvmo, T., Warren, S.G., and Zender, C.S.: Bounding  
477 the role of black carbon in the climate system: A scientific assessment, *J. Geophys.*  
478 *Res.-Atmos.*, 118, 5380-5552, doi: 10.1002/jgrd.50171, 2013.
- 479 Cachier, H., Bremond, M.P., and Buat-Menard, P.: Determination of atmospheric soot  
480 carbon with a simple thermal method, *Tellus B.*, 41, 379-390, doi: 10.1111/j.1600-  
481 0889.1989.tb00316.x, 1989.
- 482 Cachier, H. and Pertuisot, M.H.: Particulate Carbon in Arctic Ice, *Analisis*, 22, M34-  
483 M37, 1994.
- 484 Cao, J.J., Lee, S.C., Ho, K.F., Zhang, X.Y., Zou, S.C., Fung, K., Chow, J.C., and Watson, J.G.:  
485 Characteristics of carbonaceous aerosol in Pearl River Delta Region, China during  
486 2001 winter period, *Atmos. Environ.*, 37, 1451-1460, doi: 10.1016/S1352-  
487 2310(02)01002-6, 2003.
- 488 Cao, J.J., Wu, F., Chow, J.C., Lee, S.C., Li, Y., Chen, S.W., An, Z.S., Fung, K.K., Watson, J.G.,  
489 Zhu, C.S., and Liu, S.X.: Characterization and source apportionment of atmospheric  
490 organic and elemental carbon during fall and winter of 2003 in Xi'an, China, *Atmos.*  
491 *Chem. Phys.*, 5, 3127-3137, doi: 10.5194/acp-5-3127-2005, 2005.



- 492 Cao, J.J., Lee, S.C., Chow, J.C., Watson, J.G., Ho, K.F., Zhang, R.J., Jin, Z.D., Shen, Z.X., Chen,  
493 G.C., Kang, Y.M., Zou, S.C., Zhang, L.Z., Qi, S.H., Dai, M.H., Cheng, Y., and Hu, K.: Spatial  
494 and seasonal distributions of carbonaceous aerosols over China, *J. Geophys. Res.-*  
495 *Atmos.*, 112, doi: 10.1029/2006JD008205, 2007.
- 496 Carmagnola, C.M., Domine, F., Dumont, M., Wright, P., Strellis, B., Bergin, M., Dibb, J.,  
497 Picard, G., Libois, Q., Arnaud, L., and Morin, S.: Snow spectral albedo at Summit,  
498 Greenland: measurements and numerical simulations based on physical and  
499 chemical properties of the snowpack, *The Cryosphere*, 7, 1139-1160, doi:  
500 10.5194/tc-7-1139-2013, 2013.
- 501 Chen, L.W.A., Chow, J.C., Watson, J.G., Moosmuller, H., and Arnott, W.P.: Modeling  
502 reflectance and transmittance of quartz-fiber filter samples containing elemental  
503 carbon particles: Implications for thermal/optical analysis, *J. Aerosol Sci.*, 35, 765-  
504 780, doi: 10.1016/j.jaerosci.2003.12.005, 2004.
- 505 Chow, J.C., Watson, J.G., Pritchett, L.C., Pierson, W.R., Frazier, C.A., and Purcell, R.G.:  
506 The Dri Thermal Optical Reflectance Carbon Analysis System - Description,  
507 Evaluation and Applications in United-States Air-Quality Studies, *Atmos. Environ.*,  
508 27, 1185-1201, doi: 10.1016/0960-1686(93)90245-T, 1993.
- 509 Chow, J.C., Watson, J.G., Lu, Z.Q., Lowenthal, D.H., Frazier, C. A., Solomon, P. A., Thuillier,  
510 R. H., Magliano, K.: Descriptive analysis of PM(2.5) and PM(10) at regionally  
511 representative locations during SJVAQS/AUSPEX. *Atmos. Environ.*, 30, 2079-2112,  
512 doi: 10.1016/1352-2310(95)00402-5, 1996.
- 513 Chow, J.C., Watson, J.G., Crow, D., Lowenthal, D.H., and Merrifield, T.: Comparison of  
514 IMPROVE and NIOSH carbon measurements, *Aerosol Sci. Technol.*, 34, 23-34, doi:  
515 10.1080/02786820119073, 2001.
- 516 Chow, J.C., Watson, J.G., Chen, L.W.A., Arnott, W.P., Moosmuller, H., and Fung, K.:  
517 Equivalence of elemental carbon by thermal/optical reflectance and transmittance  
518 with different temperature protocols, *Environ. Sci. Technol.*, 38, 4414-4422, doi:  
519 10.1021/es034936u, 2004.
- 520 Chuang, C.C., Penner, J.E., Prospero, J.M., Grant, K.E., Rau, G.H., and Kawamoto, K.:  
521 Cloud susceptibility and the first aerosol indirect forcing: Sensitivity to black



- 522 carbon and aerosol concentrations, *J. Geophys. Res.-Atmos.*, 107, doi:  
523 10.1029/2000JD000215, 2002.
- 524 Chylek, P., Srivastava, V., Cahenzli, L., Pinnick, R.G., Dod, R.L., Novakov, T., Cook, T.L.,  
525 and Hinds, B.D.: Aerosol and Graphitic Carbon Content of Snow, *J. Geophys. Res.-*  
526 *Atmos.*, 92, 9801-9809, doi: 10.1029/JD092iD08p09801, 1987.
- 527 Clarke, A.D., Noone, K.J., Heintzenberg, J., Warren, S.G., and Covert, D.S.: Aerosol Light-  
528 Absorption Measurement Techniques - Analysis and Intercomparisons, *Atmos.*  
529 *Environ.*, 21, 1455-1465, doi: 10.1016/0004-6981(67)90093-5, 1967.
- 530 Cong, Z., Kang, S., Kawamura, K., Liu, B., Wan, X., Wang, Z., Gao, S., and Fu, P.:  
531 Carbonaceous aerosols on the south edge of the Tibetan Plateau: concentrations,  
532 seasonality and sources, *Atmos. Chem. Phys.*, 15, 1573-1584, doi: 10.5194/acp-15-  
533 1573-2015, 2015.
- 534 Cross, E.S., Onasch, T.B., Ahern, A., Wrobel, W., Slowik, J.G., Olfert, J., Lack, D.A., Massoli,  
535 P., Cappa, C.D., Schwarz, J.P., Spackman, J.R., Fahey, D.W., Sedlacek, A., Trimborn, A.,  
536 Jayne, J.T., Freedman, A., Williams, L.R., Ng, N.L., Mazzoleni, C., Dubey, M., Brem, B.,  
537 Kok, G., Subramanian, R., Freitag, S., Clarke, A., Thornhill, D., Marr, L.C., Kolb, C.E.,  
538 Worsnop, D.R., and Davidovits, P.: Soot Particle Studies-Instrument Inter-  
539 Comparison-Project Overview, *Aerosol Sci. Technol.*, 44, 592-611, 2010.
- 540 Dang, C. and Hegg, D.A.: Quantifying light absorption by organic carbon in Western  
541 North American snow by serial chemical extractions, *J. Geophys. Res.-Atmos.*, 119,  
542 10247-10261, doi: 10.1002/2014JD022156, 2014.
- 543 Doherty, S.J., Warren, S.G., Grenfell, T.C., Clarke, A.D., and Brandt, R.E.: Light-absorbing  
544 impurities in Arctic snow, *Atmos. Chem. Phys.*, 10, 11647-11680, doi: 10.5194/acp-  
545 10-11647-2010, 2010.
- 546 Doherty, S.J., Dang, C., Hegg, D.A., Zhang, R.D., and Warren, S.G.: Black carbon and other  
547 light-absorbing particles in snow of central North America, *J. Geophys. Res.-Atmos.*,  
548 119, 12807-12831, doi: 10.1002/2014JD022350, 2014.
- 549 Fischer K.: Bestimmung der Absorption von sichtbarer Strahlung durch  
550 Aerosolpartikeln, *Contr. Atmos. Phys.*, 43, 244-254, 1970.



- 551 Flanner, M.G., Liu, X., Zhou, C., Penner, J.E., and Jiao, C.: Enhanced solar energy  
552 absorption by internally-mixed black carbon in snow grains, *Atmos. Chem. Phys.*,  
553 12, 4699-4721, doi: 10.5194/acp-12-4699-2012, 2012.
- 554 Forsstrom, S., Isaksson, E., Skeie, R.B., Strom, J., Pedersen, C.A., Hudson, S.R., Berntsen,  
555 T.K., Lihavainen, H., Godtliebsen, and F., Gerland, S.: Elemental carbon  
556 measurements in European Arctic snow packs, *J. Geophys. Res.-Atmos.*, 118,  
557 13614-13627, doi: 10.1002/2013JD019886, 2013.
- 558 Gillies, J. A., Gertler, A.W., Sagebiel, J.C., Dippel, W.A.: On-road particulate matter  
559 (PM<sub>2.5</sub> and PM<sub>10</sub>) emissions in the Sepulveda Tunnel, Los Angeles, California.  
560 *Environ. Sci. Technol.*, 35, 1054-1063, 2001.
- 561 Gray, H. A., Cass, G. R., Huntzicker, J. J., Heyerdahl, E.K., Rau, J.A.: Characteristics of  
562 Atmospheric Organic and Elemental Carbon Particle Concentrations in Los-Angeles.  
563 *Environ. Sci. Technol.*, 20, 580-589, doi: 10.1021/Es00148a006, 1986.
- 564 Grenfell, T.C., Doherty, S.J., Clarke, A.D., and Warren, S.G.: Light absorption from  
565 particulate impurities in snow and ice determined by spectrophotometric analysis  
566 of filters, *Appl. Opt.*, 50, 2037-2048, doi: 10.1364/AO.50.002037, 2011.
- 567 Hadley, O.L., Corrigan, C.E., Kirchstetter, T.W., Cliff, S.S., and Ramanathan, V.:  
568 Measured black carbon deposition on the Sierra Nevada snow pack and implication  
569 for snow pack retreat, *Atmos. Chem. Phys.*, 10, 7505-7513, doi: 10.5194/acp-10-  
570 7505-2010, 2010.
- 571 Hadley, O.L. and Kirchstetter, T.W.: Black-carbon reduction of snow albedo, *Nat. Clim.*  
572 *Chang.*, 2, 437-440, doi: 10.1038/NCLIMATE1433, 2012.
- 573 Han, Y. M., Han, Z. W., Cao, J. J., Chow, J.C., Watson, J.G., An, Z.S., Liu, S.X., Zhang, R.J.:  
574 Distribution and origin of carbonaceous aerosol over a rural high-mountain lake  
575 area, Northern China and its transport significance. *Atmos. Environ.*, 42, 2405-2414,  
576 doi: 10.1016/j.atmosenv.2007.12.020, 2008.
- 577 Hansen, A. D. A., Rosen, H., and Novakov, T.: The aethalometer — An instrument for  
578 the real-time measurement of optical absorption by aerosol particles, *Sci. Total*  
579 *Environ.*, 36, 191-196, doi: 10.1016/0048-9697(84)90265-1, 1984.



- 580 Hansen, J., Sato, M., Ruedy, R., Nazarenko, L., Lacis, A., Schmidt, G.A., Russell, G., Aleinov,  
581 I., Bauer, M., Bauer, S., Bell, N., Cairns, B., Canuto, V., Chandler, M., Cheng, Y., Del  
582 Genio, A., Faluvegi, G., Fleming, E., Friend, A., Hall, T., Jackman, C., Kelley, M., Kiang,  
583 N., Koch, D., Lean, J., Lerner, J., Lo, K., Menon, S., Miller, R., Minnis, P., Novakov, T.,  
584 Oinas, V., Perlwitz, J., Perlwitz, J., Rind, D., Romanou, A., Shindell, D., Stone, P., Sun,  
585 S., Tausnev, N., Thresher, D., Wielicki, B., Wong, T., Yao, M., and Zhang, S.: Efficacy of  
586 climate forcings, *J. Geophys. Res.-Atmos.*, 110, doi: 10.1029/2005JD005776, 2005.
- 587 Heintzenberg, J.: Fine particles in the global troposphere A review, *Tellus B.*, 41, 149-  
588 160, doi: 10.1111/j.1600-0889.1989.tb00132.x, 1989.
- 589 Hitzenger, R.: Absorption-Measurements with an Integrating Plate Photometer  
590 Calibration and Error Analysis, *Aerosol Sci. Technol.*, 18, 70-84, doi:  
591 10.1080/02786829308959585, 1993.
- 592 Horvath, H.: Comparison of Measurements of Aerosol Optical-Absorption by Filter  
593 Collection and a Transmissometric Method, *Atmos. Environ.*, 27, 319-325, doi:  
594 10.1016/0960-1686(93)90105-8, 1993a.
- 595 Horvath, H.: Atmospheric Light-Absorption - a Review, *Atmos. Environ.*, 27, 293-317,  
596 doi: 10.1016/0960-1686(93)90104-7, 1993b.
- 597 Huang, J.P., Fu, Q.A., Zhang, W., Wang, X., Zhang, R.D., Ye, H., and Warren, S.G.: Dust and  
598 Black Carbon in Seasonal Snow across Northern China, *Bull. Amer. Meteor. Soc.*, 92,  
599 175-181, doi: 10.1175/2010BAMS3064.1, 2011.
- 600 IPCC. 2013. *Climate Change 2013: The Physical Science Basis*[M]. Stocker, T. F., D. Qin,  
601 G. K. Plattner, et al., Cambridge, United Kingdom and New York, NY, USA.
- 602 Ivleva, N. P., McKeon, U., Niessner, R., and Pöschl, U.: Raman microspectroscopic  
603 analysis of size-resolved atmospheric aerosol particle samples collected with an  
604 ELPI: Soot, humic-like substances, and inorganic compounds, *Aerosol Sci. Technol.*,  
605 41, 655–671, doi:10.1080/02786820701376391, 2007.
- 606 Jacobson, M.Z.: Strong radiative heating due to the mixing state of black carbon in  
607 atmospheric aerosols, *Nature* 409, 695-697, doi: 10.1038/35055518, 2001a.



- 608 Jacobson, M.Z.: Global direct radiative forcing due to multicomponent anthropogenic  
609 and natural aerosols, *J. Geophys. Res.-Atmos.*, 106, 1551-1568, doi:  
610 10.1029/2000JD900514, 2001b.
- 611 Jenk, T.M., Szidat, S., Schwikowski, M., Gaggeler, H.W., Brutsch, S., Wacker, L., Synal,  
612 H.A., and Saurer, M.: Radiocarbon analysis in an Alpine ice core: record of  
613 anthropogenic and biogenic contributions to carbonaceous aerosols in the past  
614 (1650-1940), *Atmos. Chem. Phys.*, 6, 5381-5390, doi: 10.5194/acp-6-5381-2006,  
615 2006.
- 616 Jimenez, J. L., Canagaratna, M. R., Donahue, N. M., Prevot, A.S.H., Zhang, Q., Kroll, J.H.,  
617 DeCarlo, P.F., Allan, J.D., Coe, H., Ng, N.L., Aiken, A.C., Docherty, K.S., Ulbrich, I.M.,  
618 Grieshop, A.P., Robinson, A.L., Duplissy, J., Smith, J.D., Wilson, K.R., Lanz, V.A.,  
619 Hueglin, C., Sun, Y.L., Tian, J., Laaksonen, A., Raatikainen, T., Rautiainen, J.,  
620 Vaattovaara, P., Ehn, M., Kulmala, M., Tomlinson, J.M., Collins, D.R., Cubison, M.J.,  
621 Dunlea, E.J., Huffman, J.A., Onasch, T.B., Alfarra, M.R., Williams, P.I., Bower, K., Kondo,  
622 Y., Schneider, J., Drewnick, F., Borrmann, S., Weimer, S., Demerjian, K., Salcedo, D.,  
623 Cottrell, L., Griffin, R., Takami, A., Miyoshi, T., Hatakeyama, S., Shimono, A., Sun, J.Y.,  
624 Zhang, Y.M., Dzepina, K., Kimmel, J.R., Sueper, D., Jayne, J.T., Herndon, S.C., Trimborn,  
625 A.M., Williams, L.R., Wood, E.C., Middlebrook, A.M., Kolb, C.E., Baltensperger, U.,  
626 Worsnop, D.R.: Evolution of organic aerosols in the atmosphere, *Science*, 326,  
627 1525–1529, 2009.
- 628 Koch, D., Schulz, M., Kinne, S., McNaughton, C., Spackman, J.R., Balkanski, Y., Bauer, S.,  
629 Berntsen, T., Bond, T.C., Boucher, O., Chin, M., Clarke, A., De Luca, N., Dentener, F.,  
630 Diehl, T., Dubovik, O., Easter, R., Fahey, D.W., Feichter, J., Fillmore, D., Freitag, S.,  
631 Ghan, S., Ginoux, P., Gong, S., Horowitz, L., Iversen, T., Kirkevåg, A., Klimont, Z.,  
632 Kondo, Y., Krol, M., Liu, X., Miller, R., Montanaro, V., Moteki, N., Myhre, G., Penner,  
633 J.E., Perlwitz, J., Pitari, G., Reddy, S., Sahu, L., Sakamoto, H., Schuster, G., Schwarz, J.P.,  
634 Seland, O., Stier, P., Takegawa, N., Takemura, T., Textor, C., van Aardenne, J.A., and  
635 Zhao, Y.: Evaluation of black carbon estimations in global aerosol models, *Atmos.*  
636 *Chem. Phys.*, 9, 9001-9026, doi: 10.5194/acp-9-9001-2009, 2009.



- 637 Legrand, M., Preunkert, S., Schock, M., Cerqueira, M., Kasper-Giebl, A., Afonso, J., Pio,  
638 C., Gelencser, A., and Dombrowski-Etchevers, I.: Major 20th century changes of  
639 carbonaceous aerosol components (EC, WinOC, DOC, HULIS, carboxylic acids, and  
640 cellulose) derived from Alpine ice cores, *J. Geophys. Res.-Atmos.*, 112, doi:  
641 10.1029/2006JD008080, 2007.
- 642 Li, W., Shao, L., Zhang, D., Ro, C.-U., Hu, M., Bi, X., Geng, H., Matsuki, A., Niu, H., and Chen,  
643 J.: A review of single aerosol particle studies in the atmosphere of East Asia:  
644 morphology, mixing state, source, and heterogeneous reactions, *J. Clean Prod.*, 112,  
645 1330-1349, <https://doi.org/10.1016/j.jclepro.2015.04.050>, 2016.
- 646 Lim, S., Fain, X., Zanatta, M., Cozic, J., Jaffrezo, J.L., Ginot, P., and Laj, P.: Refractory black  
647 carbon mass concentrations in snow and ice: method evaluation and inter-  
648 comparison with elemental carbon measurement, *Atmos. Meas. Tech.*, 7, 3307-  
649 3324, doi: 10.5194/amt-7-3307-2014, 2014.
- 650 McMeeking, G.R., Morgan, W.T., Flynn, M., Highwood, E.J., Turnbull, K., Haywood, J.,  
651 and Coe, H.: Black carbon aerosol mixing state, organic aerosols and aerosol optical  
652 properties over the United Kingdom, *Atmos. Chem. Phys.*, 11, 9037-9052, doi:  
653 10.5194/acp-11-9037-2011, 2011.
- 654 Menon, S., Hansen, J., Nazarenko, L., Luo, Y.F.: Climate effects of black carbon aerosols  
655 in China and India, *Science* 297, 2250-2253, doi: 10.1126/science.1075159, 2002.
- 656 Ming, J., Cachier, H., Xiao, C., Qin, D., Kang, S., Hou, S., and Xu, J.: Black carbon record  
657 based on a shallow Himalayan ice core and its climatic implications, *Atmos. Chem.*  
658 *Phys.*, 8, 1343-1352, doi: 10.5194/acp-8-1343-2008, 2008.
- 659 Ming, J., Xiao, C.D., Cachier, H., Qin, D.H., Qin, X., Li, Z.Q., and Pu, J.C.: Black Carbon (BC)  
660 in the snow of glaciers in west China and its potential effects on albedos, *Atmos.*  
661 *Res.*, 92, 114-123, doi: 10.1016/j.atmosres.2008.09.007, 2009.
- 662 Ming, J., Xiao, C.D., Sun, J.Y., Kang, S.C., and Bonasoni, P.: Carbonaceous particles in the  
663 atmosphere and precipitation of the Nam Co region, central Tibet, *J. Environ. Sci.*,  
664 22, 1748-1756, doi: 10.1016/S1001-0742(09)60315-6, 2010.



- 665 Moosmuller, H., Chakrabarty, R.K., and Arnott, W.P.: Aerosol light absorption and its  
666 measurement: A review, *J. Quant. Spectrosc. Ra.*, 110, 844-878, doi:  
667 10.1016/j.jqsrt.2009.02.035, 2009.
- 668 Moteki, N., Kondo, Y., Takegawa, N., and Nakamura, S.-i.: Directional dependence of  
669 thermal emission from nonspherical carbon particles, *J. Aerosol Sci.*, 40, 790-801,  
670 doi: 10.1016/j.jaerosci.2009.05.003, 2009.
- 671 Murphy, D. M., Cziczo, D. J., Froyd, K. D., Hudson, P. K., Matthew, B. M., Middlebrook, A.  
672 M., Peltier, R. E., Sullivan, A., Thomson, D. S., Weber, R. J.: Single-particle mass  
673 spectrometry of tropospheric aerosol particles. *J. Geophys. Res.*, 111, D23S32,  
674 doi:10.1029/2006JD007340, , 2006.
- 675 Ogren, J. A. and Charlson, R. J.: Elemental carbon in the atmosphere– cycle and lifetime,  
676 *Tellus*, 35B, 241–254, 1983.
- 677 Painter, T.H., Seidel, F.C., Bryant, A.C., Skiles, S.M., and Rittger, K.: Imaging  
678 spectroscopy of albedo and radiative forcing by light-absorbing impurities in  
679 mountain snow, *J. Geophys. Res.-Atmos.*, 118, 9511-9523, doi: 10.1002/jgrd.50520,  
680 2013.
- 681 Pan, Y.P., Wang, Y.S., Xin, J.Y., Tang, G.Q., Song, T., Wang, Y.H., Li, X.R., and Wu, F.K.:  
682 Study on dissolved organic carbon in precipitation in Northern China, *Atmos.*  
683 *Environ.*, 44, 2350-2357, doi: 10.1016/j.atmosenv.2010.03.033, 2010.
- 684 Pavese, G., Calvello, M., and Esposito, F.: Black Carbon and Organic Components in the  
685 Atmosphere of Southern Italy: Comparing Emissions from Different Sources and  
686 Production Processes of Carbonaceous Particles, *Aerosol Air Qual. Res.*, 12, 1146-  
687 1156, doi: 10.4209/aaqr.2011.12.0236, 2012.
- 688 Pedersen, C.A., Gallet, J.C., Strom, J., Gerland, S., Hudson, S.R., Forsstrom, S., Isaksson,  
689 E., and Berntsen, T. K.: In situ observations of black carbon in snow and the  
690 corresponding spectral surface albedo reduction, *J. Geophys. Res.-Atmos.*, 120,  
691 1476-1489, doi: 10.1002/2014jd022407, 2015.
- 692 Petzold, A., Kopp, C., and Niessner, R.: The dependence of the specific attenuation  
693 cross-section on black carbon mass fraction and particle size, *Atmos. Environ.*, 31,  
694 661-672, doi: 10.1016/S1352-2310(96)00245-2, 1997.





- 695 Petzold, A., Ogren, J. A., Fiebig, M., Laj, P., Li, S.-M., Baltensperger, U., Holzer-Popp, T.,  
696 Kinne, S., Pappalardo, G., Sugimoto, N., Wehrli, C., Wiedensohler, A., and Zhang, X.-  
697 Y.: Recommendations for reporting "black carbon" measurements, *Atmos. Chem.*  
698 *Phys.*, 13, 8365-8379, <https://doi.org/10.5194/acp-13-8365-2013>, 2013.
- 699 Qian, Y., Wang, H., Zhang, R., Flanner, M.G., and Rasch, P.J.: A sensitivity study on  
700 modeling black carbon in snow and its radiative forcing over the Arctic and  
701 Northern China, *Environ. Res. Lett.*, 9, 064001, doi: 10.1088/1748-  
702 9326/9/6/064001, 2014.
- 703 Quinn, P. K. and Bates, T. S.: North American, Asian, and Indian haze: Similar regional  
704 impacts on climate? *Geophys. Res. Lett.*, 30, 1555, doi:10.1029/2003GL016934,  
705 2003.
- 706 Ramanathan, V., and Carmichael, G.: Global and regional climate changes due to black  
707 carbon, *Nat. Geosci.*, 1, 221-227, Doi 10.1038/Ngeo156, 2008.
- 708 Rosenfeld, D., Lohmann, U., Raga, G.B., O'Dowd, C.D., Kulmala, M., Fuzzi, S., Reissell, A.,  
709 and Andreae, M.O.: Flood or drought: How do aerosols affect precipitation? *Science*  
710 321, 1309-1313, doi: 10.1126/science.1160606, 2008.
- 711 Schmid, H., Laskus, L., Abraham, H.J., Baltensperger, U., Lavanchy, V., Bizjak, M., Burba,  
712 P., Cachier, H., Crow, D., Chow, J., Gnauk, T., Even, A., ten Brink, H.M., Giesen, K.P.,  
713 Hitzenberger, R., Hueglin, C., Maenhaut, W., Pio, C., Carvalho, A., Putaud, J.P., Toom-  
714 Saunty, D., and Puxbaum, H.: Results of the "carbon conference" international  
715 aerosol carbon round robin test stage I, *Atmos. Environ.*, 35, 2111-2121, doi:  
716 10.1016/S1352-2310(00)00493-3, 2001.
- 717 Schwarz, J.P., Doherty, S.J., Li, F., Ruggiero, S.T., Tanner, C.E., Perring, A.E., Gao, R.S.,  
718 and Fahey, D.W.: Assessing Single Particle Soot Photometer and Integrating  
719 Sphere/Integrating Sandwich Spectrophotometer measurement techniques for  
720 quantifying black carbon concentration in snow, *Atmos. Meas. Tech.*, 5, 2581-2592,  
721 doi: 10.5194/amt-5-2581-2012, 2012.
- 722 Sharma, S., Brook, J.R., Cachier, H., Chow, J., Gaudenzi, A., and Lu, G.: Light absorption  
723 and thermal measurements of black carbon in different regions of Canada, *J.*  
724 *Geophys. Res.-Atmos.*, 107, doi: 10.1029/2002JD002496, 2002.



- 725 Slater, J.F., Currie, L.A., Dibb, J.E., and Benner, B.A.: Distinguishing the relative  
726 contribution of fossil fuel and biomass combustion aerosols deposited at Summit,  
727 Greenland through isotopic and molecular characterization of insoluble carbon,  
728 *Atmos. Environ.*, 36, 4463-4477, doi: 10.1016/S1352-2310(02)00402-8, 2002.
- 729 Spencer, M.T., Shields, L.G., and Prather, K. A.: Simultaneous measurement of the  
730 effective density and chemical composition of ambient aerosol particles, *Environ.*  
731 *Sci. Technol.*, 41, 1303-1309, doi:10.1021/es061425+, 2007.
- 732 Thevenon, F., Anselmetti, F.S., Bernasconi, S.M., and Schwikowski, M.: Mineral dust  
733 and elemental black carbon records from an Alpine ice core (Colle Gnifetti glacier)  
734 over the last millennium, *J. Geophys. Res.-Atmos.*, 114, doi:  
735 10.1029/2008JD011490, 2009.
- 736 Turpin, B. J., Cary, R. A., and Huntzicker, J. J.: An insitu,time-resolved analyzer for  
737 aerosol organic and elemental carbon. *Aerosol Sci. Technol.*, 12, 161-171, doi:  
738 10.1080/02786829008959336, 1990.
- 739 Turpin, B. J., and Huntzicker, J. J.: Secondary formation of organic aerosol in the Los  
740 Angeles Basin: A descriptive analysis of organic and elemental carbon  
741 concentrations. *Atmos. Environ.*, 25A, 207-215, 1991.
- 742 von Schneidmesser, E., Schauer, J.J., Hagler, G.S.W., and Bergin, M.H.: Concentrations  
743 and sources of carbonaceous aerosol in the atmosphere of Summit, Greenland,  
744 *Atmos. Environ.*, 43, 4155-4162, doi: 10.1016/j.atmosenv.2009.05.043, 2009.
- 745 Wang, M., Xu, B., Zhao, H., Cao, J., Joswiak, D., Wu, G., and Lin, S.: The Influence of Dust  
746 on Quantitative Measurements of Black Carbon in Ice and Snow when Using a  
747 Thermal Optical Method, *Aerosol Sci. Technol.*, 46, 60-69, doi:  
748 10.1080/02786826.2011.605815, 2012.
- 749 Wang, X., Doherty, S.J., and Huang, J.P.: Black carbon and other light-absorbing  
750 impurities in snow across Northern China, *J. Geophys. Res.-Atmos.*, 118, 1471-1492,  
751 doi: 10.1029/2012JD018291, 2013.
- 752 Wang, X., Pu, W., Ren, Y., Zhang, X.L., Zhang, X.Y., Shi, J.S., Jin, H.C., Dai, M.K., Chen, Q.L.:  
753 Observations and model simulations of snow albedo reduction in seasonal snow



- 754 due to insoluble light-absorbing particles during 2014 Chinese survey, *Atmos.*  
755 *Chem. Phys.*, 17, 2279-2296, doi: 10.5194/acp-17-2279-2017, 2017.
- 756 Wang, R, Tao, S., Balkanski, Y., Ciais, P., Boucher, O., Liu, J.F., Piao, S.L., Shen, H.Z., Vuolo,  
757 M.R., Valari, M., Chen, H., Chen, Y.C., Cozic, A., Huang, Y., Li, B.A., Li, W., Shen, G.F.,  
758 Wang, B., Zhang, Y.Y.: Exposure to ambient black carbon derived from a unique  
759 inventory and high-resolution model. *Proc. Natl. Acad. Sci. USA.*, 111, 2459-2461,  
760 doi: 10.1073/pnas.1318763111, 2014.
- 761 Watson, J. G., and Chow, J. C.: Comparison and evaluation of in situ and filter carbon  
762 measurements at the Fresno Supersite, *J. Geophys. Res.-Atmos.*, 107,  
763 doi:10.1029/2001jd000573, 2002.
- 764 Wolff, E.W. and Cachier, H.: Concentrations and seasonal cycle of black carbon in  
765 aerosol at a coastal Antarctic station, *J. Geophys. Res.-Atmos.*, 103, 11033-11041,  
766 doi: 10.1029/97JD01363, 1998.
- 767 Xu, B.Q., Yao, T.D., Liu, X.Q., and Wang, N.L.: Elemental and organic carbon  
768 measurements with a two-step heating-gas chromatography system in snow  
769 samples from the Tibetan Plateau, *Annals of Glaciology*, Vol 43, 2006 43, 257-262,  
770 doi: 10.3189/172756406781812122, 2006.
- 771 Xu, B.Q., Cao, J.J., Hansen, J., Yao, T.D., Joswia, D.R., Wang, N.L., Wu, G.J., Wang, M., Zhao,  
772 H.B., Yang, W., Liu, X.Q., and He, J.Q.: Black soot and the survival of Tibetan glaciers,  
773 *Proc. Nat. Acad. Sci. U.S.A.*, 106, 22114-22118, doi: 10.1073/pnas.0910444106,  
774 2009a.
- 775 Xu, B.Q., Wang, M., Joswiak, D.R., Cao, J.J., Yao, T.D., Wu, G.J., Yang, W., and Zhao, H.B.:  
776 Deposition of anthropogenic aerosols in a southeastern Tibetan glacier, *J. Geophys.*  
777 *Res.-Atmos.*, 114, doi: 10.1029/2008JD011510, 2009b.
- 778 Xu, B.Q., Cao, J.J., Joswiak, D.R., Liu, X.Q., Zhao, H.B., and He, J.Q.: Post-depositional  
779 enrichment of black soot in snow-pack and accelerated melting of Tibetan glaciers,  
780 *Environ. Res. Lett.*, 7, doi: 10.1088/1748-9326/7/1/014022, 2012.
- 781 Yang, H., and Yu, J.Z.: Uncertainties in charring correction in the analysis of elemental  
782 and organic carbon in atmospheric particles by thermal/optical methods, *Environ.*  
783 *Sci. Technol.*, 36, 5199-5204, doi: 10.1021/es025672z, 2002.



784 Yasunari, T. J., Tan, Q., Lau, K. M., Bonasoni, P., Marinoni, A., Laj, P., Menegoz, M.,  
785 Takemura, T., and Chin, M.: Estimated range of black carbon dry deposition and the  
786 related snow albedo reduction over Himalayan glaciers during dry pre-monsoon  
787 periods, *Atmos. Environ.*, 78, 259-267, doi:10.1016/j.atmosenv.2012.03.031, 2013.  
788 Yasunari, T. J., Koster, R. D., Lau, W. K. M., Kim, K.: Impact of snow darkening via dust,  
789 black carbon, and organic carbon on boreal spring climate in the Earth system. *J.*  
790 *Geophys. Res.-Atmos.*, 120, 5485-5503, doi: 10.1002/2014jd022977, 2015.  
791 Ye, H., Zhang, R.D., Shi, J.S., Huang, J.P., Warren, S.G., and Fu, Q.: Black carbon in  
792 seasonal snow across northern Xinjiang in northwestern China, *Environ. Res. Lett.*,  
793 7, doi: 10.1088/1748-9326/7/4/044002, 2012.  
794 Zhang, R.J., Ho, K.F., Cao, J.J., Han, Z.W., Zhang, M.G., Cheng, Y., and Lee, S.C.: Organic  
795 carbon and elemental carbon associated with PM10 in Beijing during spring time,  
796 *J. Hazard. Mater.*, 172, 970-977, doi: 10.1016/j.jhazmat.2009.07.087, 2009.  
797 Zhao, C., Hu, Z., Qian, Y., Leung, L.R., Huang, J., Huang, M., Jin, J., Flanner, M.G., Zhang,  
798 R., Wang, H., Yan, H., Lu, Z., and Streets, D.G.: Simulating black carbon and dust and  
799 their radiative forcing in seasonal snow: a case study over North China with field  
800 campaign measurements, *Atmos. Chem. Phys.*, 14, 11475-11491, doi: 10.5194/acp-  
801 14-11475-2014, 2014  
802 Zhou, Y., Wang, X., Wu, X.Q., Cong, Z.Y., Wu, G.M., Ji, M.X.: Quantifying Light Absorption  
803 of Iron Oxides and Carbonaceous Aerosol in Seasonal Snow across Northern China,  
804 *Atmosphere-Basel*, 8, doi: 10.3390/atmos8040063, 2017.  
805  
806



807 **Figure captions:**

808 Figure 1 Sampling locations. Sites 90–102 are located in northeast China and were used for snow sample  
809 collection during Jan–Feb. 2014. Snow sampling site 103 is located in Lanzhou in northwest China, and  
810 was used for atmospheric sample collection during 5–25 August 2015. Sites are numbered according to  
811 Wang et al. (2013) and Ye et al. (2012).

812 Figure 2 Schematic diagram of the improved two-sphere integrating spectrophotometer.

813 Figure 3 Calibration curve for standard fullerene soot at a wavelength of 600 nm. The solid line is a  
814 best-fit curve for the filter measurements.  $S_0$  and  $S$  are the detected signals for the blank and sample  
815 filters, respectively, and  $-\ln(S/S_0)$  is the relative attenuation.

816 Figure 4 Comparison of the theoretical and measured BC mass determined by the TSI and two-step  
817 techniques in the laboratory. The solid and dot–dashed lines represent best-fit lines for the TSI and two-  
818 step techniques, respectively. The dashed line is a 1:1 line.

819 Figure 5 Mass loss of standard fullerene soot on 1.0- $\mu\text{m}$  quartz fiber filters determined by refiltration  
820 using 0.4- $\mu\text{m}$  Nuclepore filters.

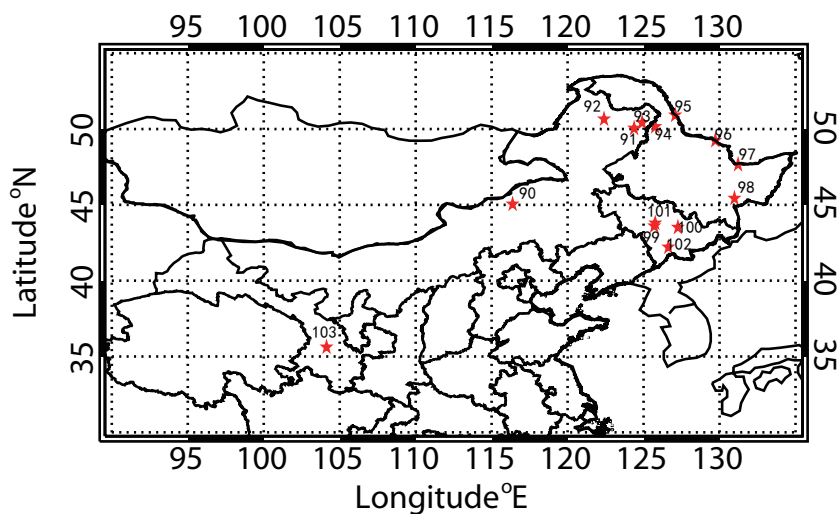
821 Figure 6 Comparison of BC concentrations in snow samples over northeast China during January–  
822 February 2014 determined by the TSI and two-step thermal optical methods. A 1:1 line (dashed) and a  
823 linear regression fit passing through the origin (solid curve) are also shown.

824 Figure 7 As for Fig. 6, but for atmospheric samples collected at Lanzhou in northwest China during 5–  
825 25 August 2015.

826 Figure 8 Spatial distributions of light absorption due to BC and non-BC fractions in surface snow across  
827 northern China during January–February 2014.



828 Figure 9 Variations in 8-hour (a) BC concentration and (b) BC and non-BC light absorption measured  
829 by TSI spectrophotometer at Lanzhou during 5–25 August 2015 (day: 9 am to 5 pm; night: 11 pm to 7  
830 am).  
831



832

833 **Figure 1** Sampling locations. Sites 90–102 are located in northeast China and were used  
834 for snow sample collection during Jan–Feb. 2014. Snow sampling site 103 is located in  
835 Lanzhou in northwest China, and was used for atmospheric sample collection during 5–25  
836 August 2015. Sites are numbered according to Wang et al. (2013) and Ye et al. (2012).

837



838 **Table 1** Series of 15 standard filters loaded with fullerene soot, and a comparison of BC  
 839 concentrations between theoretical calculations and the TSI/two-step thermal–optical  
 840 methods in the laboratory.

Filter	Standard BC Concentration ( $\mu\text{g}/\text{cm}^2$ )	Filter	Standard BC Concentration ( $\mu\text{g}/\text{cm}^2$ )	Filter	Calculated BC ( $\mu\text{g}$ )	TSI BC ( $\mu\text{g}$ )	Two-step BC ( $\mu\text{g}$ )
1	0.63	9	2.82	1	3.68	3.92	2.28
2	0.70	10	3.65	2	10.58	11.39	5.86
3	0.78	11	5.53	3	17.48	17.49	11.39
4	0.86	12	6.35	4	24.38	24.94	15.67
5	0.93	13	12.5	5	31.28	32.52	18.07
6	1.33	14	19.00	6	38.18	39.14	24.29
7	2.12	15	38.6	7	45.08	49.18	28.61
8	2.49	-	-	-	-	-	

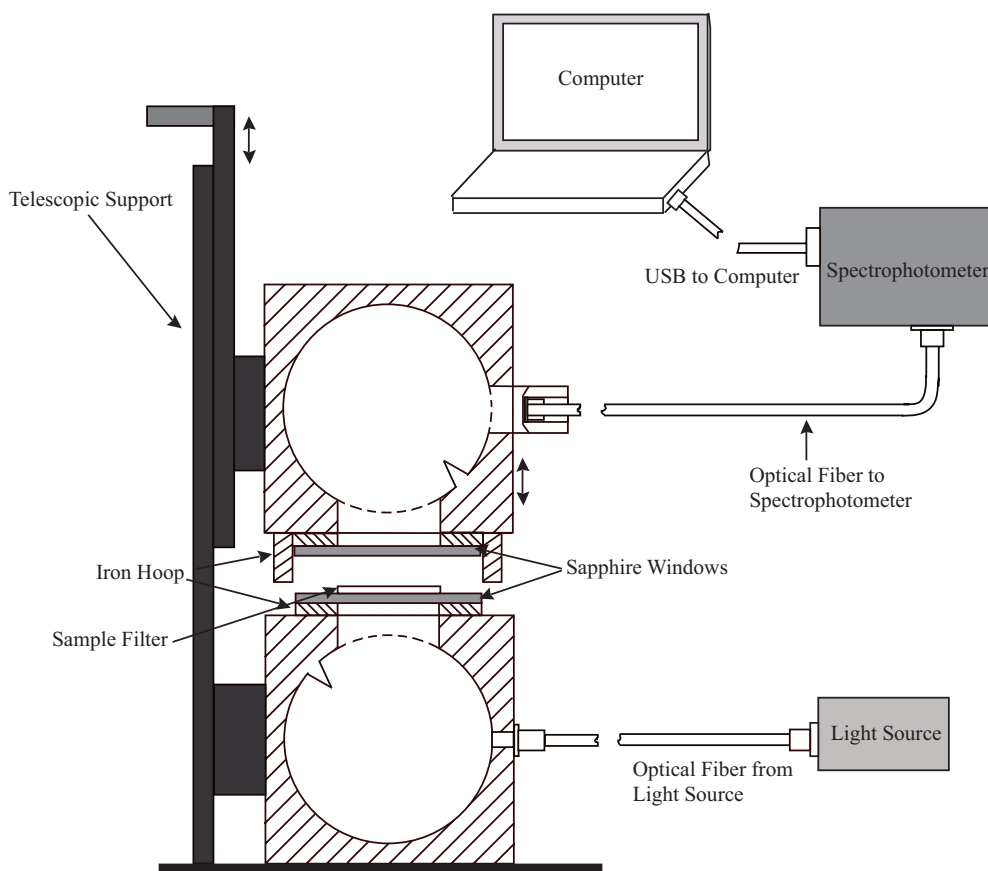
841

842





843  
844  
845  
846

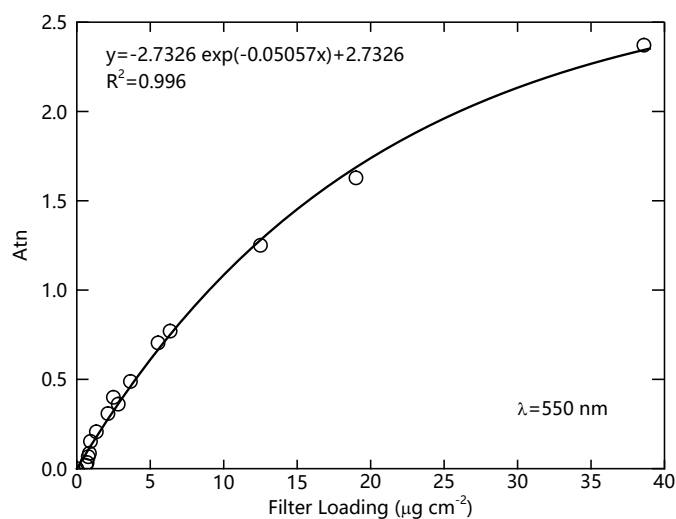


847  
848  
849  
850  
851  
852  
853  
854  
855

**Figure 2** Schematic diagram of the improved two-sphere integrating spectrophotometer.



856  
857  
858  
859  
860  
861

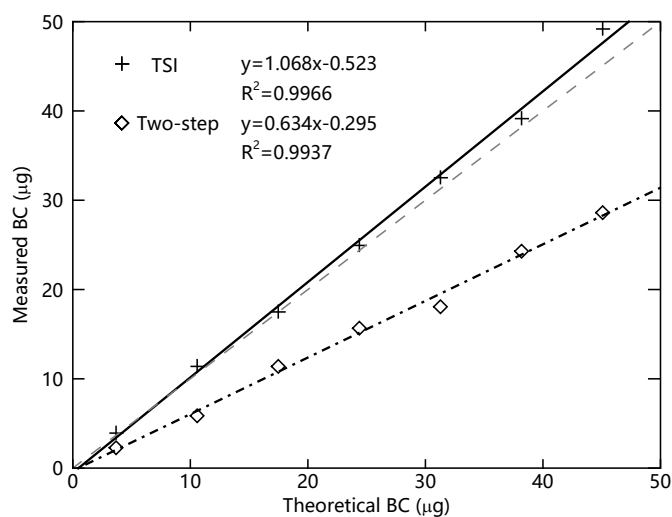


862  
863  
864  
865  
866

**Figure 3** Calibration curve for standard fullerene soot at a wavelength of 600 nm. The solid line is a best-fit curve for the filter measurements.  $S_0$  and  $I$  are the detected signals for the blank and sample filters, respectively, and  $-\ln(S/S_0)$  is the relative attenuation.



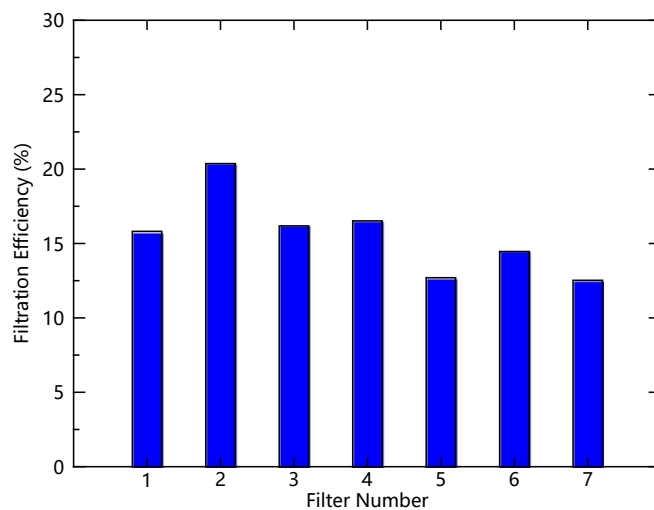
867  
868  
869  
870  
871  
872



873  
874 **Figure 4** Comparison of the theoretical and measured BC mass determined by the TSI and  
875 two-step techniques in the laboratory. The solid and dot-dashed lines represent best-fit  
876 lines for the TSI and two-step techniques, respectively. The dashed line is a 1:1 line.  
877



878  
879  
880  
881  
882  
883



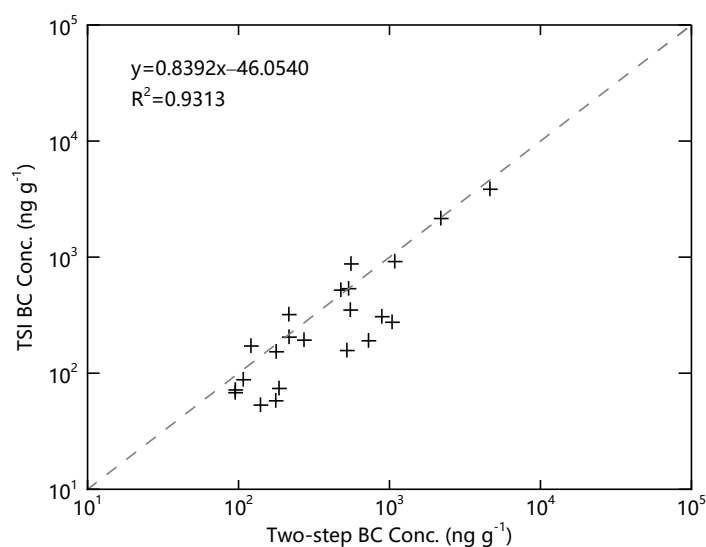
884  
885 **Figure 5** Mass loss of standard fullerene soot on 1.0- $\mu\text{m}$  quartz fiber filters determined by  
886 refiltration using 0.4- $\mu\text{m}$  Nuclepore filters.  
887



888

889

890



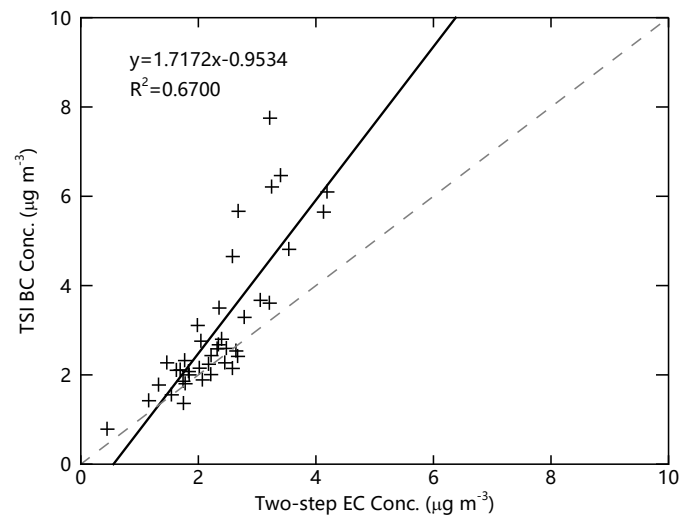
891

892 **Figure 6** Comparison of BC concentrations in snow samples over northeast China during  
893 January–February 2014 determined by the TSI and two-step thermal optical methods. A  
894 1:1 line (dashed) and a linear regression fit passing through the origin (solid curve) are also  
895 shown.

896



897  
898  
899  
900  
901



902  
903 **Figure 7** As for Fig. 6, but for atmospheric samples collected at Lanzhou in northwest  
904 China during 5–25 August 2015.  
905



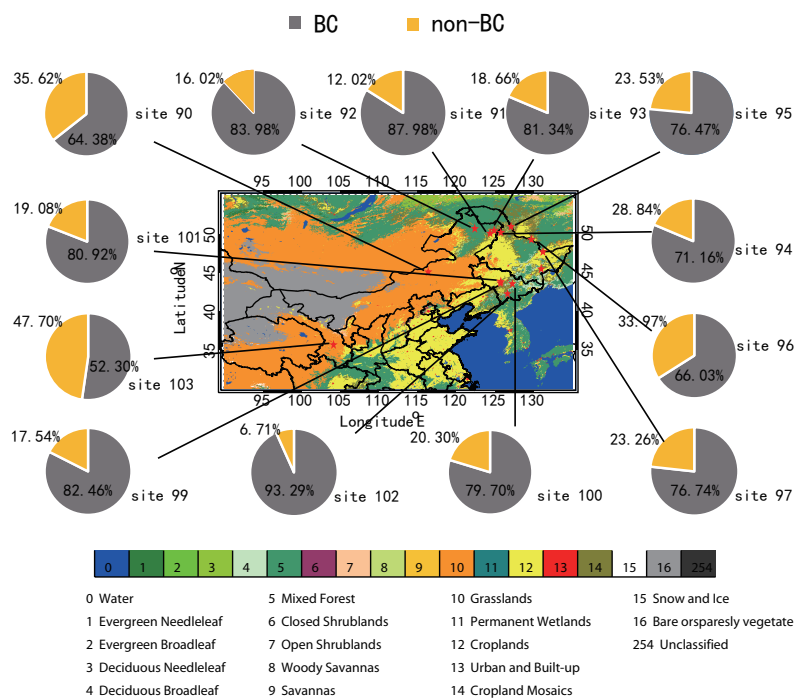
906 **Table 2** Statistics of BC and EC concentrations measured using the TSI and two-step  
907 thermal–optical methods for snow samples during the experiments over northern China.  
908  
909

Site	Filter	TSI BC	Two-step EC
		ng g <sup>-1</sup>	ng g <sup>-1</sup>
90	Q-351L	349.95	550.19
91	Q-352L	171.46	120.87
	Q-352R	152.94	177.48
92	Q-354L	53.10	139.78
	Q-354R	57.82	176.41
93	Q-356L	71.71	95.27
	Q-356R	73.85	185.45
94	Q-358L	274.62	1040.20
95	Q-359L	87.84	107.51
	Q-359R	67.92	95.01
96	Q-363L	319.71	215.42
	Q-363R	192.60	271.42
97	Q-366L	204.47	216.04
	Q-366R	306.75	889.54
98	Q-369L	1605.95	130.36
	Q-369R	1321.69	6004.33
99	Q-376L	873.58	555.39
	Q-376R	534.70	536.11
100	Q-380R	519.47	476.14
101	Q-384R	3843.15	4626.72
102	Q-388L	915.59	1083.24
	Q-388R	2151.18	2187.90
103	Q-397L	156.76	522.07
	Q-397R	190.24	726.08



910

911



912

913 **Figure 8** Spatial distributions of light absorption due to BC and non-BC fractions in surface  
 914 snow across northern China during January–February 2014.

915

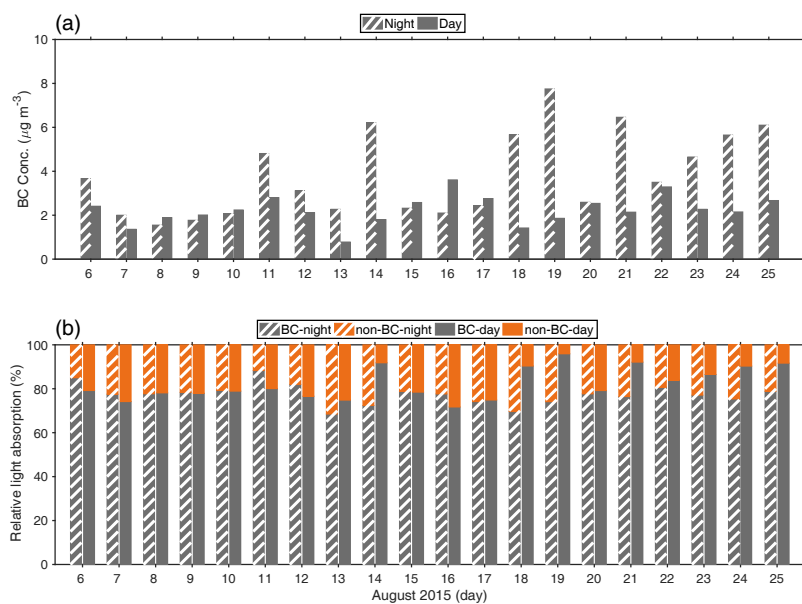




916

917

918



919

920 **Figure 9** Variations in 8-hour (a) BC concentration and (b) BC and non-BC light  
921 absorption measured by TSI spectrophotometer at Lanzhou during 5–25 August 2015 (day:  
922 9 am to 5 pm; night: 11 pm to 7 am).

923



924

925 **Table 3** Statistics of BC and EC concentrations in atmospheric samples measured using  
 926 the TSI and two-step thermal–optical methods.

927

Day			Night		
Date	TSI BC	Two-step EC	Date	TSI BC	Two-step EC
	$\mu\text{g m}^{-3}$	$\mu\text{g m}^{-3}$		$\mu\text{g m}^{-3}$	$\mu\text{g m}^{-3}$
2015. 8. 6	2. 41	2. 67	2015. 8. 5–8. 6	3. 67	3. 05
2015. 8. 7	1. 36	1. 75	2015. 8. 6–8. 7	2. 00	1. 84
2015. 8. 8	1. 89	2. 07	2015. 8. 7–8. 8	1. 55	1. 54
2015. 8. 9	2. 01	2. 21	2015. 8. 8–8. 9	1. 77	1. 32
2015. 8. 10	2. 24	2. 17	2015. 8. 9–8. 10	2. 07	1. 83
2015. 8. 11	2. 80	2. 40	2015. 8. 10–8. 11	4. 81	3. 54
2015. 8. 12	2. 11	1. 69	2015. 8. 11–8. 12	3. 11	1. 98
2015. 8. 13	0. 78	0. 45	2015. 8. 13–8. 14	2. 27	1. 46
2015. 8. 14	1. 80	1. 78	2015. 8. 14–8. 15	6. 21	3. 25
2015. 8. 15	2. 58	2. 32	2015. 8. 15–8. 16	2. 32	1. 77
2015. 8. 16	3. 61	3. 21	2015. 8. 16–8. 17	2. 10	1. 63
2015. 8. 17	2. 76	2. 04	2015. 8. 17–8. 18	2. 43	2. 22
2015. 8. 18	1. 42	1. 15	2015. 8. 18–8. 19	5. 66	2. 68
2015. 8. 19	1. 86	1. 74	2015. 8. 19–8. 20	7. 75	3. 21
2015. 8. 20	2. 54	2. 64	2015. 8. 20–8. 21	2. 59	2. 48
2015. 8. 21	2. 14	2. 58	2015. 8. 21–8. 22	6. 46	3. 40
2015. 8. 22	3. 29	2. 78	2015. 8. 22–8. 23	3. 50	2. 35
2015. 8. 23	2. 27	2. 45	2015. 8. 23–8. 24	4. 65	2. 58
2015. 8. 24	2. 15	2. 02	2015. 8. 24–8. 25	5. 65	4. 13
2015. 8. 25	2. 67	2. 34	2015. 8. 25–8. 26	6. 10	4. 19

928